2018

Investigations of Automatic Meshing in Modeling a Dry Twin Screw Compressor

David Henry Rowinski
Convergent Science, Inc., United States of America, david.rowinski@convergecfd.com

Yanheng Li
Convergent Science, Inc., United States of America, yanheng.li@convergecfd.com

Karan Bansal
Convergent Science, Inc., United States of America, karan.bansal@convergecfd.com

Investigations of Automatic Meshing in Modeling a Dry Twin Screw Compressor

David ROWINSKI[1]*, Yanheng LI[1], Karan BANSAL[1]

[1]Convergent Science, Inc.
Madison, WI, USA
david.rowinski@convergecfd.com

* Corresponding Author

ABSTRACT

In order to design screw compressors for optimal performance, it is crucial to understand the complex fluid flow processes within them. Computational fluid dynamics (CFD) is one approach for doing so. Considerable progress has been made over the last several years in both commercial and academic solution packages for this application; however, due to the complex moving geometries of the screw rotors and the tight clearances between the moving parts, a major challenge that remains is the generation of numerical grids that are increasingly efficient, accurate, robust, and easily created. In this study, an alternate methodology for this problem is presented. The grid is created automatically at every time step based on the instantaneous geometry using a Cartesian cut-cell based method which preserves exactly the changing control volume shapes. Automatic mesh refinement is employed to adaptively increase mesh resolution where the flow variables have large gradients in order to resolve the large-scale flow structures. To address the problem of efficiently modeling the flows in the small clearance gaps, an empirical model is applied so that the cells within the gaps can remain relatively coarse. This removes a major bottleneck from the computational cost and allows more mesh resolution to be applied in accurately capturing the physics of the port flows. The effect of the thermal expansion on the gap sizes is accounted for by considering the heat transfer from the fluid to the solid walls and then periodically solving the solid to steady state using cycle-averaged heat transfer coefficients; the clearances therefore vary throughout the length of the rotors. The model is validated against experimental measurements of the internal pressure, mass flow rate, temperature, and power for two operating conditions. A global grid convergence study demonstrates the spatial and temporal convergence of the numerical model, and establishes necessary computational costs for varying levels of accuracy. It is shown that for the tested configurations, numerically accurate results are achieved with a total turn-around time that is low enough for practical use in engineering applications.

1. INTRODUCTION

Twin screw compressors are important devices for providing pressurized gases in industrial, manufacturing, and refrigeration applications, to name a few. Their basic principle of operation involves two counter-rotating helical screws which form chambers whose volumes decrease as the screws rotate. The gas is pressurized as the volume decreases, and it then exits from the chambers as a discharge port is exposed. The efficiency of these devices is strongly affected by the fluid dynamics of the flow through the ports, by the leakage flows that occur between chambers, and by the mechanical and thermal deformation of the components. In order to design these types of compressors for optimal efficiency, models for the fluidic and thermodynamic processes are invaluable.

Chamber models, which model the thermodynamic processes in zero-dimensional or one-dimensional context of the individual compression flow path components, have been developed in the past several decades in the works by Stostic (1988), Kauder (1994), Hanjalic (1997), and Janicki (2007). These models offer a concise description of the thermodynamic processes, and their elegance and simplicity makes them ideal for engineering use with relatively little computational effort required. However, as simplified models, they have limitations in their use especially in dealing with unique aspects of the interaction between the flow and the geometry.

Computational fluid dynamics (CFD) offers designers a complete description of a modeled three-dimensional transient flow path through a solution of modeled transport equations for mass, momentum, and energy. This requires the fluid volume to be discretized into a numerical grid on which the equations are solved. The geometric complexity of screw compressors, including the helical rotors, small gaps between rotors and housing, complex sealing surfaces, port shapes, and their evolution in time makes the direct application of traditional CFD approaches difficult for these devices. Several approaches have been taken to this problem, the predominant one being analytical grid generation based methods, as developed in Kovacevic (2002), further developed in Rane (2013), and demonstrated in the context of the arbitrary Lagrangian Eulerian (ALE) framework in Voorde Vande (2005). Many applications of these or similar methods have been used in CFD models of screw machines, including work in investigating port flows of Sauls (2009), Kethidi (2011), Pascu (2013), Kovacevic (2014), Arjeneh (2015), as well as modeling internal pressure in screw compressors by Kovacevic (2014) and in screw expanders by Rainer (2016).

The aforementioned approaches to CFD modeling of screw compressors can be further improved upon in several regards. First is the reduction of computational cost, which can render various approaches difficult to apply in an engineering context or limit the areas in which cell resolution can be affordably increased. Second is the generality, in which some of the methods place constraints on the allowable geometries. Some alternate approaches include the application of the overset mesh method, as applied in a screw compressor using a commercial CFD solver in Byeon (2017). Additionally, work has been performed in the coupling between chamber models and finite-element analysis (FEA) tools as applied to screw expanders in Nikolov (2012), and coupling between chamber models and CFD applied to screw vacuum pumps in Lu (2017). In this work, however, a different approach is investigated to retain the details of the three dimensional flow in the model.

This work demonstrates the application of a Cartesian cut-cell based mesh to the CFD modeling of twin screw compressors. The meshing strategy has several advantages, including its ease in applicability to general geometries, highly orthogonal cells for high accuracy and stability, and use of adaptive mesh refinement to add resolution automatically in large gradients. The primary challenge in the application of this method is the computationally feasible treatment of the leakage flows, which are very important in this application. To address this problem, a simplified model is introduced to model the leakage flows instead of fully resolving them. This removes a major bottleneck from the computational cost and presents the opportunity to resolve more fully the chamber interior and port flows. The work concludes by addressing the grid discretization error, validating for an experimentally measured compressors, and presenting strategies to balance cost and accuracy for practical engineering use.

2. METHODOLOGY

The CFD methodology used in this work is based on that shown in Senecal (2007) and Richards (2017) and available in the commercial software package CONVERGE. This involves dynamic mesh generation which is very tightly coupled to the solution of the governing equations. Defining the mesh begins with a triangulated surface that bounds the fluid. A Cartesian orthogonal mesh is defined in the interior based on a user-specified base grid size. At the boundaries, where the orthogonal cells are intersected by the triangulated bounding surface, cut-cells that take the form of arbitrary-sided polyhedra are formed. An example of the mesh for a twin screw compressor is shown

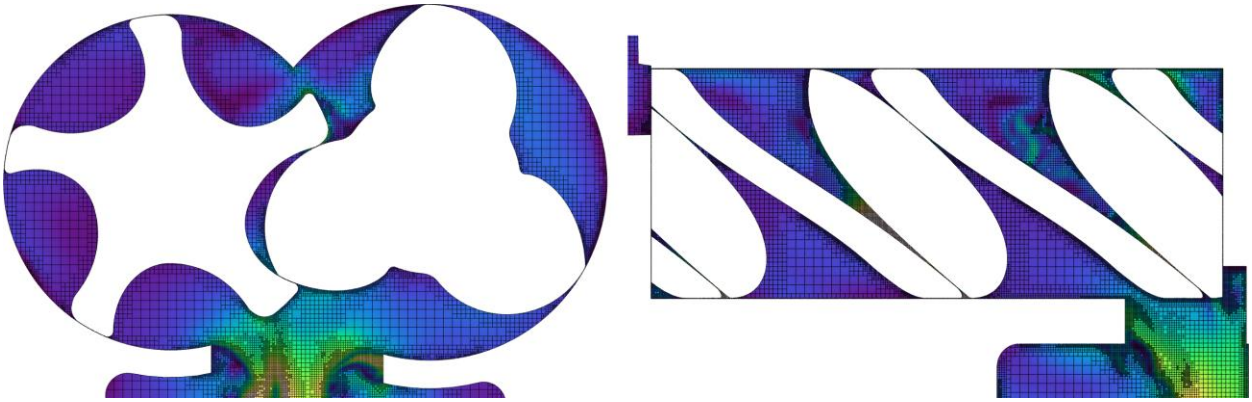

Figure 1: General demonstration of the cut-cell based mesh with adaptive mesh refinement applied to a dry twin screw compressor. The planes are colored by velocity and mesh lines are overlaid.

below in Figure 1. The boundary cells exchanges flux with their neighbors, and at the boundaries they receive flux based on the boundary conditions. Movement of any boundary can be incorporated simply by moving the triangulated surface. As the triangulated surface moves, polygons are swept in each boundary cell to account for the changes in volume, mass, and energy in each cell. In this way, the flow solver is inherently coupled to the mesh. This coupling allows a fully conservative finite-volume solution of the governing equations of conservation of mass, momentum, and energy. Because the cells are all stationary, there is no numerical diffusion associated with mesh movement as there is with methods that rely on a moving mesh. Adaptive mesh refinement is used to add cells where the gradients in velocity or temperature is large in the same way as in Pomraning (2014). The governing equations are solved in finite-volume form on the mesh with all variables collocated at the cell center. The Pressure Implicit with Splitting of Operators (PISO) method based on that of Issa (1985) for pressure-velocity coupling. The spatial discretization in this work is second-order for velocity and energy and first-order for turbulence quantities, and a first-order fully implicit time discretization scheme is used for stability. The Courant-Friedrichs-Lewy (CFL) numbers based on cell size, velocity, speed of sound, and diffusivity dictate the time step.

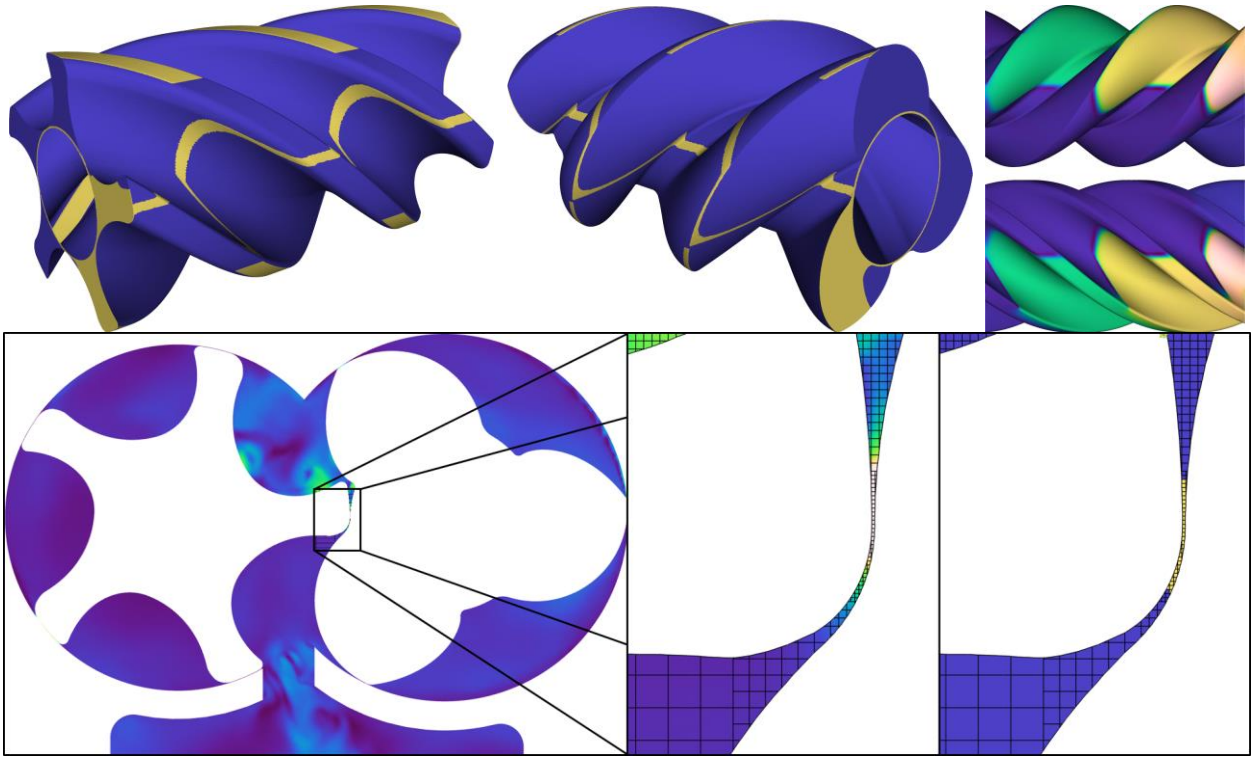

Figure 2: Description for modeling flows in small gaps. On the top left and center are the female and male rotors colored by proximity. Blue (darker) is non-adjacent, and tan (lighter) are within the threshold gap. On the top right are the rotors colored by pressure. On the bottom row is a zoomed in view of one of the many small clearances detected in the model. In the bottom left and center, cells are colored by velocity; on the bottom right, cells are colored by proximity.

While the use of adaptive mesh refinement allows increased cell resolution throughout the domain, the length scale disparities between the gap heights and device length scale make it computationally prohibitive to fully resolve the gap flow in most practical twin screw compressors. To this end, a model is employed both to detect the under-resolved areas and to model the flow in those cells. The first step is the detect of small gaps. A K-D tree is used for a fast binary search for polygon-to-polygon distance to locate boundary cells which are with a certain tolerance from one another. Figure 2 shows the rotor surfaces colored at the location meeting the proximity tolerance, which is approximately the sealing lines between rotors and between the rotors and housing. Figure 2 also shows the mesh in a zoomed in region around one of the rotor-to-rotor clearances, and the cells within the proximity tolerance flagged.

Once the cells in the gaps have been identified, a correction is applied to the under-resolved flow so that it yields roughly the same mass flow rate through the gap as in a fully resolved mesh. This correction is made in the form of

a momentum sink, as in the same way as a porous medium. Two-dimensional flow studies are conducted on gaps of varying clearance height, length, pressure gradient, and density to examine the relationships between the form of the momentum source term and the underlying non-dimensional flow parameters such as Reynolds number and Mach number. Some typical results of these studies are shown in Figure 3 for a single orientation.

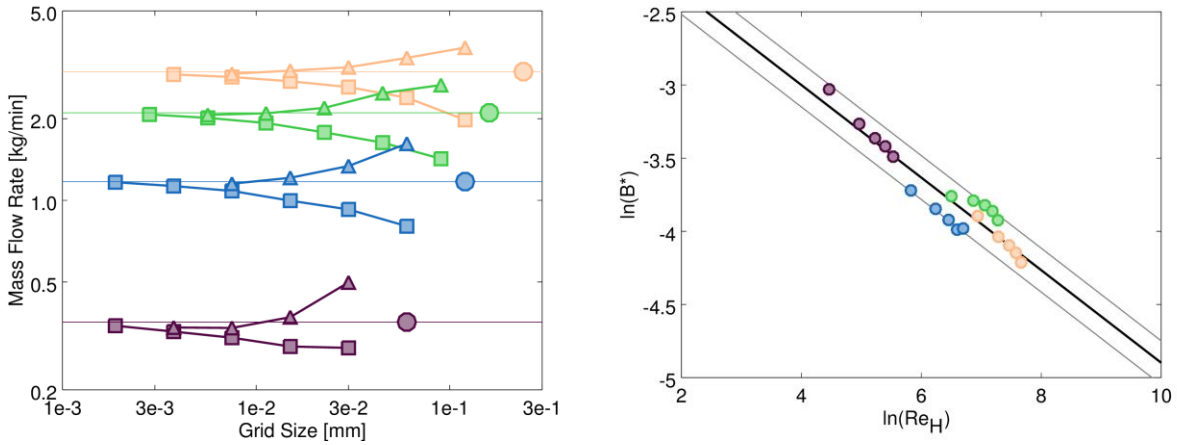

Figure 3: Results of two-dimensional gap flow studies with varying clearance height, pressure gradient, orientation, and length. To the left is the mass flow rate as a function of grid size for no-slip wall boundary conditions (squares), law-of-the-wall (triangles), and gap model (circles). To the right is the non-dimensionalized momentum source as a function of the gap Reynolds number along with the curve fit used in the simplified model.

Most of the geometry and flow configurations examined yielded a non-dimensionalized source term (B^* in Figure 3) which scaled inversely proportional to the local Reynolds number (Re_H) based on the gap height. This correlation was used to compute the momentum source term added in all of the detected under-resolved gaps. In all of the tests, the proximity tolerance was taking to be twice the physical clearance.

3. TEST CASE DESCRIPTION

The CFD model described in the previous sections is applied to a dry twin screw compressor studied experimentally and numerically by Kovacevic (2014) and Arjeneh (2015). A diagram of the fluid volume studied is shown below in Figure 4. The flow enters the compressor through the suction port (A) and is compressed by the counter-rotation of the female (B) and male (A) rotors until it exits through the discharge port (D). The rotor configuration is a 3-5 type, with three lobes on the male rotor and five lobes on the female rotor. The built-in volume ratio is 1.8, the working fluid is air, and the speed of the male rotor varies from 6,000 to 14,000 rpm. The mass flow rate, power, discharge temperature, and the inter-lobe pressure at three locations are measured for male rotor speeds of 6,000 to 8,000 rpm.

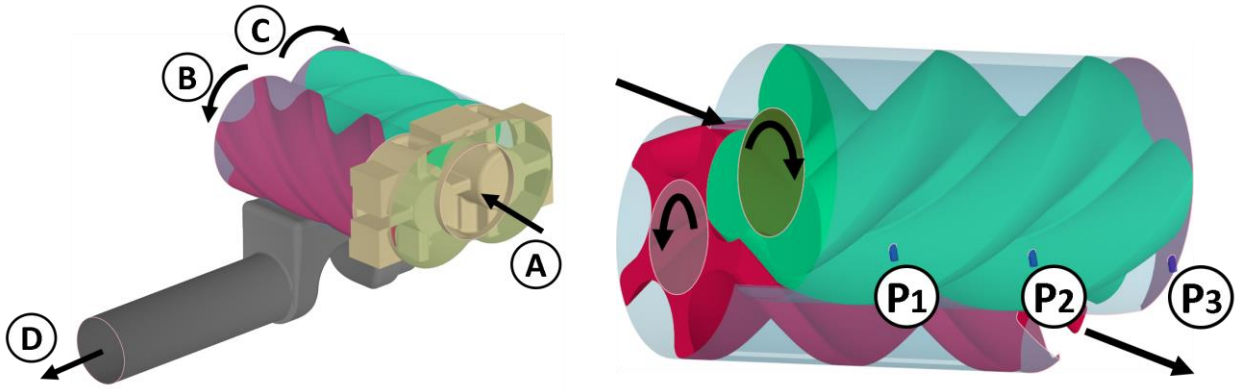

Figure 4: Picture of compressor fluid domain. The suction inlet (A), female rotor (B), male rotor (C), and discharge outlet (D) are included. On the right are the inter-lobe pressure transducers: P1, P2, and P3.

4. MODEL RESULTS AND DISCUSSION

Because the actual gap height is critical to the CFD model, the flow is first solved together with the rotor solids. The simulation begins on a coarser grid (Grid 3 from Table 1) which can run quickly and advances for 10 full revolutions of the male rotor (30 lobe passings). Throughout this time, the rotor temperatures are periodically solved to steady state using the cycle-average heat transfer coefficients and near wall temperatures to accelerate the temporal convergence. The mass flow rate stabilizes at the inlet and outlet (computed over a five-cycle average), and the rotors reach steady state temperature after about 15 lobe passings, as shown in Figure 5.

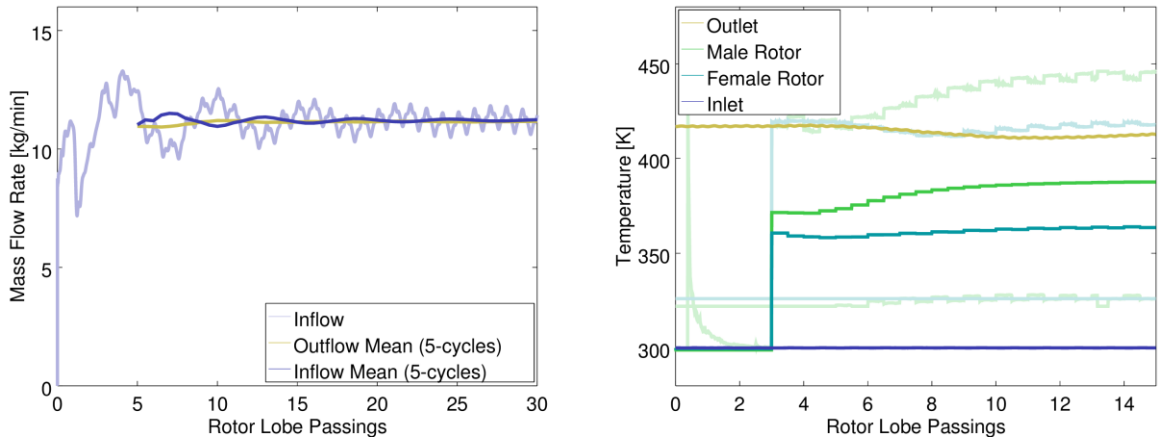

Figure 5: Evolution of mass flow rate (left) and fluid and rotor solid temperatures (right) to a stationary state.

Once the steady-state solid temperatures are reached, the thermal expansion of each rotor is estimated along its length assuming linear expansion and a thermal expansion coefficient of 12×10^{-6}. This augments the minimum rotor-to-rotor clearance from about 160 micron to 70 micron at the discharge end, and from about 160 micron to 140 micron at the suction end. The housing deformation, however, is not taken into account. From the resulting fluid state after 30 cycles on the coarse grid, the solution is mapped to begin the fluid-only simulations including the mapped rotor wall temperatures. Plots of the inter-lobe pressure compared to the measurements for the base case are shown in Figure 6 for the two rotor speeds examined. These results represent the best-practices solution methodology, including the calibrated gap model, adequate resolution, and rotor deformation.

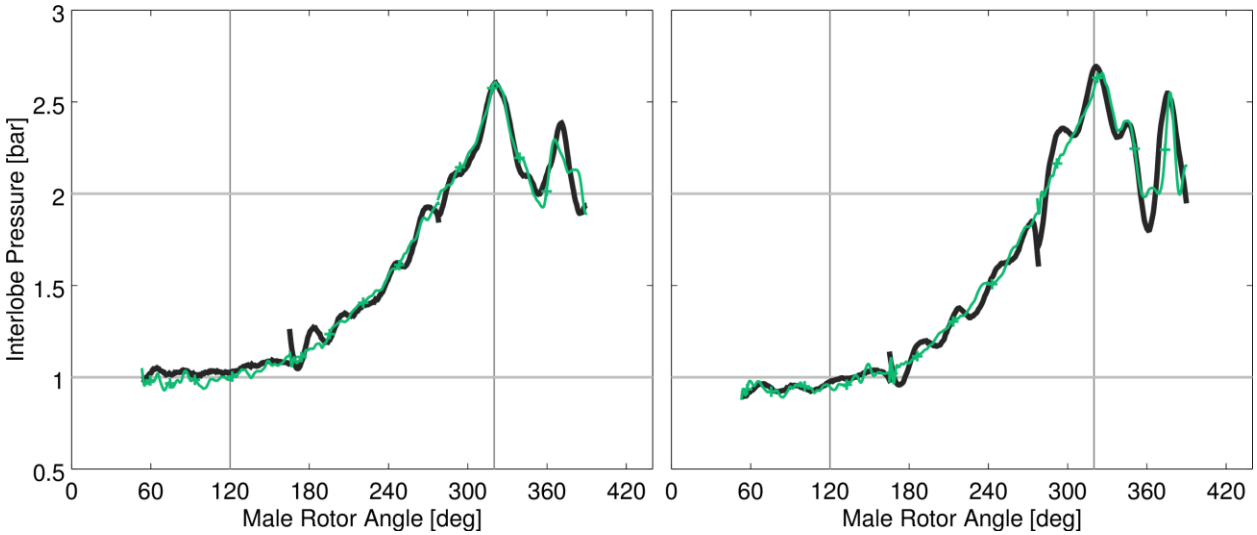

Figure 6: Measured (black solid lines) and modeled (green hatched lines) inter-lobe pressure traces for male rotor speeds of 6000 rpm (left) and 8000 rpm (right).

The results shown in Figure 6 have several notable points. First is that the pressure oscillations occurring between 60-120 degrees at both speeds could only be reproduced in the model with the inclusion of the suction pipe and a fluctuation at the same frequency applied to the inlet boundary condition. Secondly, the oscillations between 320-400 degrees were found to be sensitive to both the mesh and the outlet boundary condition. In the end, a more detailed flow path with the heat exchanger and additional discharge pipe and orifice produced results slightly more aligned with the measurements.

A major question about any CFD model is the impact of the numerical mesh resolution on the result. Global grid convergence studies were conducted so that the mesh refinement was proportional in all variations, and a single parameter controlling the base grid size was varied. Figure 7 shows some quantitative results of the mesh examination. The mass flow rate, power, and temperature do show some sensitivities to the mesh even at the finest level examined. However, note that the grid count shown in Figure 7 is plotted on a log scale, showing that the changes made in the grid size are quite extreme, spanning two orders of magnitude. Generally the global results are better for the 6000 rpm speed than for the 8000 rpm speed, however the variation is small compared to the other uncertainties which may affect these values. The mass flow rate is one of the more sensitive parameters to the mesh size, varying as much as 5% between the different grids. This is likely an affect of the gap model applicability for very large cell sizes. There is certainly deviation in the source term shown in Figure 3, and even so this model did not examine some of the more extreme limits on the grid coarseness in the gaps.

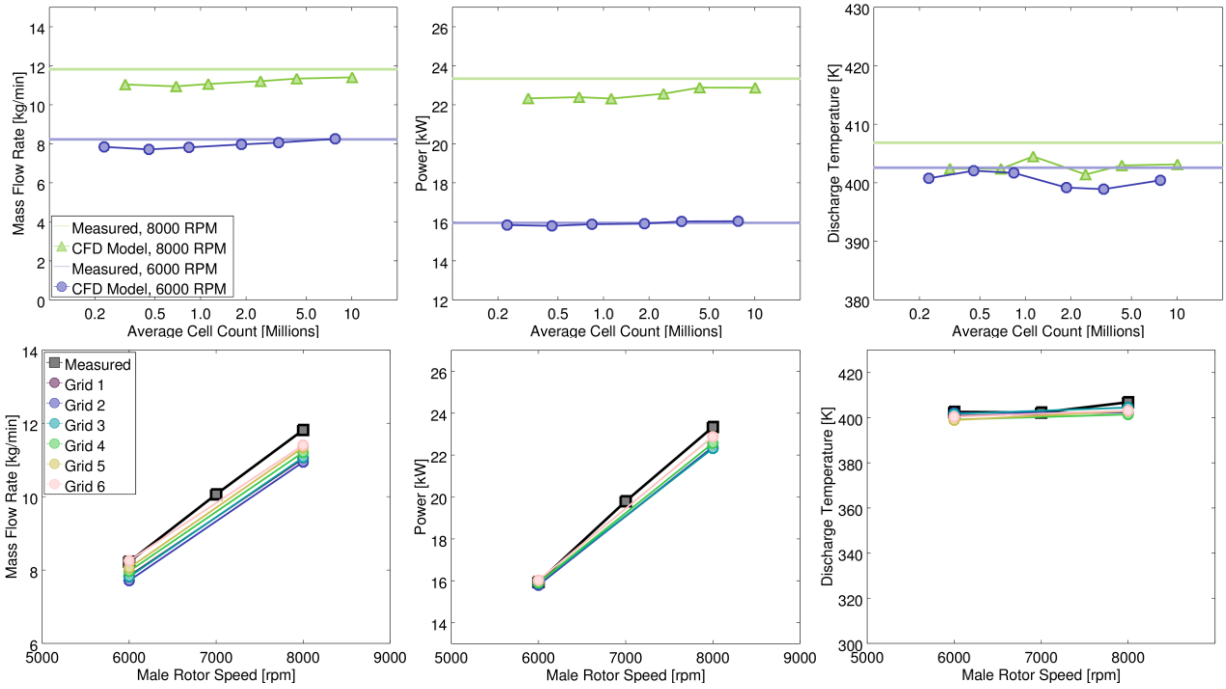

Figure 7: Figures of the mass flow rate (left), power (center), and discharge temperature (right). The top row shows the 6000 rpm (blue circles) and 8000 rpm (green triangles) results as functions of cell count. The bottom row shows measurements (black squares) and grids (from dark to light, grids 1 through 6) as functions of rotor speed.

A more qualitative look at the effect of different grids is shown in Figure 8. One fact clear from the pressure distribution on the rotors is that a slight difference is evident around the gaps for the coarsest grids, which may explain the small differences in the power. The adaptive mesh refinement captures the large-scale flow structures well, even on the coarser grids, which contributes to the cost-saving impact of this feature. One of the most interesting aspects of this method, compared to others applied to similar cases, is that similar numbers of cells may be used, but the distribution in space is very different. Here, we see a large portion of the cells contribute to resolving the flow in the discharge port and capturing the vortices and separation that occur during the discharge process. The flow from the blowhole, evident in the bottom of Figure 8 at the bottom cusp, is not fully resolved by

any means, even on the finest grids, however the effect of the mass transfer through this opening is evident in each succeeding pocket.

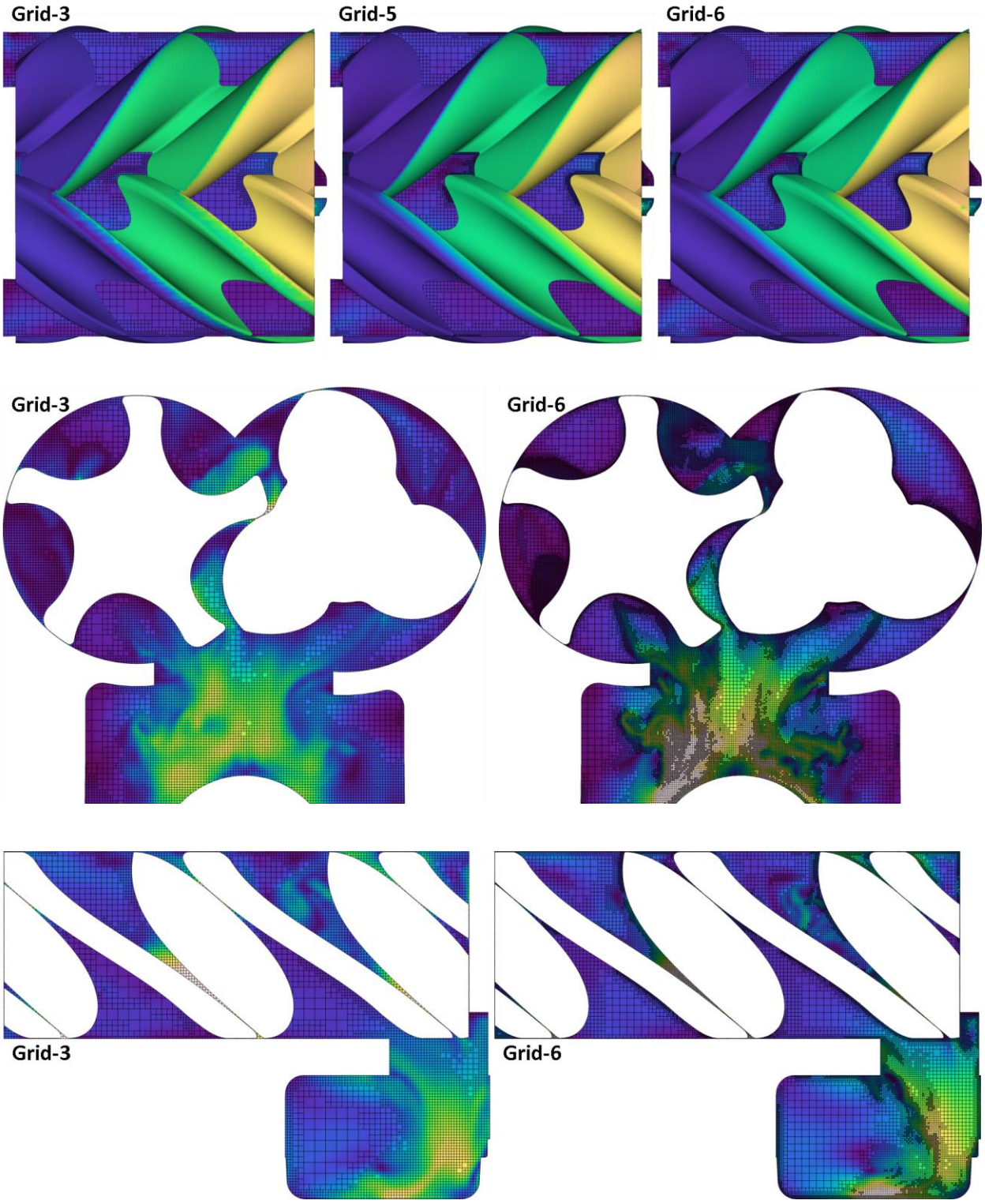

Figure 8: Visualizations from a selection of the grids investigated. The top row shows grids 3, 5, and 6 with a cut-plane colored by velocity and rotor surfaces colored by pressure. The center row shows the rotor cross section colored by velocity for grids 3 and 6. The bottom row shows the plane along the housing cusp colored by velocity.

Table 1 below provides a quantitative summary of the six different grids studied including the influence on the run time. Note that for the coarsest grids, the time step was limited differently than the other runs, so the run time appears higher than normal. As the male rotor speed increases from 6000 to 8000 rpm, the velocity gradients get larger and more adaptive mesh refinement is utilized, which increases the cost. However, since the time step is controlled by the CFL number and the leakage rates between the chambers should essentially be the same for each speed, the 6000 rpm cases can require more time steps per rotor cycle. Based on Table 1, the CFD models can be used at costs as low as 5 hours per rotor cycle, as long as the user is willing to accept an accuracy penalty of roughly 5%. However, these costs need to consider the operating condition, as generally higher pressure differentials, slower rotational speeds, smaller gaps, and more complex rotor shapes will contribute to additionally higher costs.

Table 1: Results of the grid examination for the six grids at two different speeds

	6000 RPM					*8000 RPM*				
	Mass Flow	**Power**	**Cells**	**Cycle Time**	**Time Steps**	**Mass Flow**	**Power**	**Cells**	**Cycle Time**	**Time Steps**
	kg/min	**kW**	**10^6**	**hr**	**/deg**	**kg/min**	**kW**	**10^6**	**hr**	**/deg**
Grid 1	7.84	15.83	0.2	5.5	13	11.04	22.33	0.3	4.6	10
Grid 2	7.71	15.79	0.5	5.5	13	10.94	22.39	0.7	5.2	10
Grid 3	7.82	15.87	0.8	4.8	8	11.07	22.32	1.1	5.5	6
Grid 4	7.97	15.99	1.9	11.0	13	11.21	22.56	2.5	11.1	11
Grid 5	8.06	16.02	3.3	14.3	16	11.34	22.88	4.3	23.3	13
Grid 6	8.25	16.03	7.8	60.4	40	11.40	22.87	10.7	59.9	33
Measured	8.23	15.95	--	--	--	11.82	23.34	--	--	--

A last note about the grid dependence is demonstrated in Figure 9. Here the inter-lobe pressure traces are compared for different grids. Generally, as the grid is refined, two changes occur. First, the pressure peaks become more pronounced. While the frequency is not affected as much, the peaks can vary as much as 0.2 bar. Secondly, the pressure fluctuation that is observed experimentally during compression begins to become evident in the model. The frequency is very similar between the two, but in the 8000 rpm case, the phasing is off. This is possibly due to the inlet boundary condition, and may require even more resolution or higher-order spatial schemes.

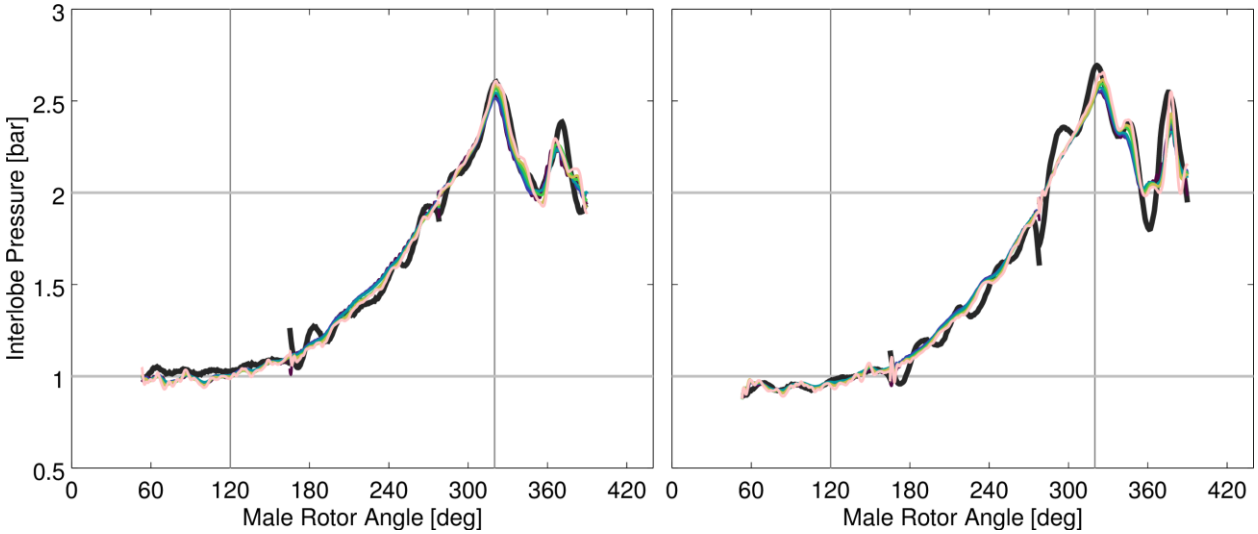

Figure 9: Measured (black solid lines) and modeled inter-lobe pressure traces for male rotor speeds of 6000 rpm (left) and 8000 rpm (right) for the grids in Table 1. The grids are colored from dark (grid 1) through light (grid 6).

5. CONCLUSIONS AND FUTURE WORK

This work has shown the application of an alternate grid generation method to model a dry twin screw compressor. While the model does require special treatment of the flows in small gaps for practical run times, it does offer some unique advantages compared to other methods. The governing equations are solved in a fully conservative approach, the stationary mesh reduces numerical diffusion, orthogonal cells yield high accuracy and stability, and adaptive mesh refinement allows the computational effort to be focused on where the internal flow or port flow velocity and temperature gradients are the highest. The mesh distribution is quite different than that produced by other grid generation methods, and the global grid convergence study is simple to perform.

With the major bottleneck of the resolution of gap flow eliminated, run times that are of practical use in engineering applications are readily achieved for a real compressor as validated here; however, users do need to be careful of how the cost can scale with the geometry and operating condition variations. Whether or not this method is of use depends on the target to be achieved. For example, if the end goal of the simulation is to examine precisely the boundary layer profiles in the gaps, this type of method will have larger computational cost. On the other hand, if the purposes of the CFD models are to examine porting configurations, pressure fluctuations, or geometry variations, this type of model is readily applicable.

REFERENCES

Andres, R., Hesse, J., Babic, H., Salecker, U., Spille-Kohoff, A., Nikolov, A., Brümmer, A. (2016). CFD Simulation of a Twin Screw Expander including Leakage Flows. *Proceedings of the 22rd International Compressor Engineering Conference at Purdue* (Paper 2497). West Lafayette, USA: Purdue University.

Arjeneh, M., Kovacevic, A., Rane, S., Manolis, M., Stosic, N. (2015). Numerical and Experimental Investigation of Pressure Losses at Suction of a Twin Screw Compressor. *Proceedings of the 9th International Conference on Compressors and their Systems*. London, UK: City University London.

Byeon, S. S., Lee, J. Y., Kim, Y. J. (2017). Performance Characteristics of 4x6 Oil-Free Twin-Screw Compressor. *Energies 2017*, 10, 945.

Hanjalic, K., Stosic, N. (1997). Development and Optimization of Screw machines with a simulation Model – Part II: Thermodynamic Performance Simulation and Design Optimization. *Transactions of the ASME 664, Vol. 119.*

Issa, R. I. (1985). Solution of the Implicitly Discretised Fluid Flow Equations by Operator-Splitting. *Journal of Computational Physics*, 62.

Janicki, M. (2007). Modellierung. und Simulation von Rotationsverdrängermaschinen. *Dissertation, TU Dortmund University, Dortmund, Germany.*

Kauder, K., Rau, B. (1994). Auslegungsverfahren fur Schraubenkompressoren. (Design Procedure for screw compressors). *VDI Berichte 1135, S. 31-44, Düsseldorf: VDI-Verlag.*

Kethidi, M., Kovacevic, A., Stosic, N., Smith, I. K. (2011). Evaluation of various turbulence models in predicting screw compressor flow processes by CFD. *Proceedings of the 7th International Conference on Compressors and their Systems*. London, UK: City University London.

Kovacevic A. (2002). Three-Dimensional Numerical Analysis for Flow Prediction in Positive Displacement Screw Machines. *Ph.D. Thesis, School of Engineering and Mathematical Sciences, City University London, UK.*

Kovacevic, A., Arjeneh, M., Rane, S., Stosic, N., Gavaises, M. (2014). Flow Visualisaton at Suction of a Twin Screw Compressor. *Proceedings of the International Conference on Screw Machines.* Dortmund, Germany: TU Dortmund.

Kovacevic, A., Rane, S., Stosic, N., Jiang, Y., Furmanczyk, M., Lowry, S. (2014). Influence of approaches in CFD Solvers on Performance Prediction in Screw Compressors. *Proceedings of the 22rd International Compressor Engineering Conference at Purdue* (Paper 2252). West Lafayette, USA: Purdue University.

Lu, Y., Fu, Y., Guo, B., Fu, L., Zhang, Q., Chen, X. (2017). Numerical Simulation of the Working Process in the Twin Screw Vacuum Pump. *Proceedings of the 10th International Conference on Compressors and their Systems*. London, UK: City University London.

Nikolov, A., Huck, C., Brümmer, A. (2012). Influence of Thermal Deformation on the Characteristic Diagram of a Screw Expander in Automotive Application of Exhaust Heat Recovery. *Proceedings of the 22rd International Compressor Engineering Conference at Purdue* (Paper 2128). West Lafayette, USA: Purdue University.

Pascu, M., Heiyanthuduwage, M., Mounoury, S., Howden Compressors Ltd. (2013). Influence of the suction arrangement and geometry of the inlet port on the performance of twin screw compressors. *Proceedings of the 8th International Conference on Compressors and their Systems*. London, UK: City University London.

Pomraning, E., Richards, K., and Senecal, P. (2014). Modeling Turbulent Combustion Using a RANS Model, Detailed Chemistry, and Adaptive Mesh Refinement. *SAE Technical Paper 2014-01-1116.*

Rane, S., Kovacevic, A., Stosic, N., Kethidi, M. (2013). CFD grid generation and analysis of screw compressor with variable geometry rotors. *Proceedings of the 8th International Conference on Compressors and their Systems*. London, UK: City University London.

Richards, K. J., Senecal, P. K., Pomraning, E. (2017). CONVERGE 2.4 Manual, Convergent Science, Madison, WI.

Sauls, J., Branch, S. (2009). CFD analysis of refrigeration screw compressors. *Proceedings of the 6th International Conference on Compressors and their Systems*. London, UK: City University London.

Senecal, P. K., Pomraning, E., Richards, K. J., Briggs, T. E., Choi, C. Y., McDavid, R. M., Patterson, M. A., Hou, S., & Shethaji, T. (2007). A New Parallel Cut-Cell Cartesian CFD Code for Rapid Grid Generation Applied to In-Cylinder Diesel Engine Simulations. SAE Technical Paper, #2007-01-0159.

Stosic, N., Kovacevic, A., Hanjalic, K., Milutinovic, L. (1988). Mathematical Modelling of the Oil Influence Upon the Working Cycle of Screw Compressors. *Proceedings of the International Compressor Engineering Conference at Purdue* (Paper 645). West Lafayette, USA: Purdue University.

Voorde Vande, J.; Vierendeels, J.; Dick, E. (2004). Development of a Laplacian-based mesh generator for ALE calculations in rotary volumetric pumps and compressors. *Comput. Methods Appl. Mech. Eng., 193, 4401–4415.*

ACKNOWLEDGEMENTS

The authors express their gratitude to Dr. Sham Rane and Professor Ahmed Kovacevic at City University London for sharing the compressor geometry and experimental measurements, and for helpful discussion on the model set up and analysis.